2020 American Control Conference
Denver, CO, USA, July 1-3, 2020

Free Energy Principle Based State and Input Observer Design for Linear Systems with Colored Noise

Ajith Anil Meera[1] and Martijn Wisse [2]

***Abstract*— The free energy principle from neuroscience provides a biologically plausible solution to the brain's inference mechanism. This paper reformulates this theory to design a brain-inspired state and input estimator for a linear time-invariant state space system with colored noise. This reformulation for linear systems bridges the gap between the neuroscientific theory and control theory, therefore opening up the possibility of evaluating it under the hood of standard control approaches. Through rigorous simulations under colored noises, the observer is shown to outperform Kalman Filter and Unknown Input Observer with minimal error in state and input estimation. It is tested against a wide range of scenarios and the proof of concept is demonstrated by applying it on a real system.**

I. INTRODUCTION

The design of state and input observer is vital towards the development of advanced industrial controllers, especially in the field of fault detection and correction [1]. Although a wide range of observer designs have been proposed for linear time invariant (LTI) systems, they assume the noises to be temporally uncorrelated (white) [2, 3]. This assumption is often violated in practice [4], resulting in a sub-optimal estimation [5]. An interesting approach called the Free Energy Principle (FEP) [6] is emerging from neuroscience, which leverages the noise smoothness in brain signals for perception. FEP demonstrates a potential to solve the problem of sub-optimal estimation. Therefore, it is imperative to reformulate it into an observer design and rigorously test it on real control system problems.

According to FEP proposed by Karl Friston, the brain's inference mechanism is a gradient descent over its free energy, where free energy is the information-theoretic measure that bounds the brain's sensory surprisal [7]. FEP emerges as a unified brain theory [8] by providing a mathematical description of brain functions [9], unifying action and perception [10], connecting physiological constructs like memory, attention, value, reinforcement and salience [9], and remaining consistent with Freudian ideas[11]. Similarities of FEP with reinforcement learning [12], neural networks [7, 13] and active learning [10] open up possibilities for biologically plausible control system techniques.

Dynamic Expectation Maximization (DEM) [14] is an interesting variant of FEP, that performs estimation on the brain's states, parameters and hyperparameters. Unlike point estimators like Kalman Filter (KF), DEM models the states in generalized coordinates and tracks the evolution of its trajectory. This renders DEM with a capability to gracefully handle coloured noise [14]. Considering that most noises in nature like wind are the product of dynamic systems - and hence coloured - it is imperative for filters to incorporate coloured noise. Moreover, the optimality of KF is affected as the noise turns coloured [15]. Many approaches have been proposed to modify KF to handle these colored noises: state augmentation and measurement differencing. State augmentation methods transform the system equations with colored noise into an equivalent higher order system with white noise before estimation [16]. However, the computations involved are sometimes ill-conditioned, and hence, other approaches like measurement differencing [17] were proposed. In this approach, the signal is whitened by subtracting the colored part from it. A detailed summary of these methods is provided in [18] and [19]. However, these methods model only causal noises and do not perform input estimation. Although few methods have been proposed for simultaneous state and input estimation, they do not handle colored noise [3, 20]. This paper aims to bridge these research gaps.

Although, FEP based tools like active inference have found applications in robotics [21, 22], there is a gap in literature for the applications of DEM [14] in control theory, which can be attributed to the relatively formidable mathematics combined with a lack of rigorous testing of DEM for LTI systems. This paper aims to bridge this gap by simplifying DEM for an LTI system and introducing a state observer design. The core contributions of the paper are:

1) the formulation of a brain inspired linear observer design for LTI system, based on DEM.
2) the extensive evaluation of the observer in simulation and its validation using a real LTI system.

II. PROBLEM STATEMENT

Consider the linear plant dynamics given in Equation 1 where A, B and C are constant system matrices, $\mathbf{x} \in \mathbb{R}^n$ is the hidden state, $\mathbf{v} \in \mathbb{R}^r$ is the input and $\mathbf{y} \in \mathbb{R}^m$ is the output.

$$\dot{\mathbf{x}} = A\mathbf{x} + B\mathbf{v} + \mathbf{w}, \qquad \mathbf{y} = C\mathbf{x} + \mathbf{z}. \tag{1}$$

Here $\mathbf{w} \in \mathbb{R}^n$ and $\mathbf{z} \in \mathbb{R}^m$ represent the process and measurement noise respectively. Variables of the plant are denoted in boldface, while its estimates are denoted in non-boldface. The noises in this paper are generated through the convolution of white noise with a Gaussian filter.

Two problems are considered in this paper. The first one is an observer design with known inputs $\mathbf{v}$, and the second one is with unknown inputs for which both x and v are to be

[1,2] are with the Department of Cognitive Robotics, TU Delft, The Netherlands. Corresponding author: ajitham1994@gmail.com.

estimated. We show that DEM outperforms KF and Unknown Input Observer (UIO) [3] for these problems respectively.

III. PRELIMINARIES

To lay the foundation of our observer design, this section introduces the key concepts and terminologies behind DEM.

A. Generative model

The key idea behind DEM to deal with coloured noise is to model the trajectory of the states using generalized coordinates. The states are expressed in generalized coordinates using its higher order derivatives as $\tilde{x} = [x\ x'\ x''\ ...]^T$. The variables in generalized coordinates are denoted by a tilde, and its components (higher derivatives) are denoted by primes. The evolution of states is written as:

$$\begin{aligned} x' &= Ax + Bv + w & y &= Cx + z \\ x'' &= Ax' + Bv' + w' & \dot{y} &= Cx' + z' \\ ... & & ... & \end{aligned} \tag{2}$$

The coloured noises are modelled to be analytic such that the covariance of noise derivatives $\tilde{z} = [z, z', z'', ...]^T$ and $\tilde{w} = [w, w', w'', ...]^T$ are well defined. The generative model representing the system is compactly written as:

$$\dot{\tilde{x}} = D_x\tilde{x} = \tilde{A}\tilde{x} + \tilde{B}\tilde{v} + \tilde{w} \qquad \tilde{y} = \tilde{C}\tilde{x} + \tilde{z} \tag{3}$$

where $D_x = \begin{bmatrix} 0 & 1 & & & \\ & 0 & 1 & & \\ & & . & . & \\ & & & 0 & 1 \\ & & & & 0 \end{bmatrix}_{(p+1)\times(p+1)} \otimes I_{n\times n}$

performs derivative operation, equivalent to shifting up all components in generalized coordinates by one block. Similar definition holds for D_v (appears later) with size $r(d+1) \times r(d+1)$, where p and d are the order of generalized motion of states and inputs respectively. Here, $\tilde{A} = I_{p+1} \otimes A$, $\tilde{B} = I_{p+1} \otimes B$ and $\tilde{C} = I_{p+1} \otimes C$, where $\otimes$ is the Kronecker tensor product.

B. Colored noise

DEM uses generalized coordinates, which models a correlation between noise derivatives through the temporal precision matrix S (inverse of covariance matrix) [14]. The correlation is assumed to be due to a Gaussian filter with S given by:

$$S(\sigma^2) = \begin{bmatrix} 1 & 0 & -\frac{1}{2\sigma^2} & .. \\ 0 & \frac{1}{2\sigma^2} & 0 & .. \\ -\frac{1}{2\sigma^2} & 0 & \frac{3}{4\sigma^4} & .. \\ .. & .. & .. & .. \end{bmatrix}^{-1}_{(p+1)\times(p+1)} \tag{4}$$

where σ^2 is the variance of Gaussian filter, with σ denoting the noise smoothness. While $\sigma^2 = 0$ denotes white noise, non-zero σ^2 denotes coloured noise. The covariance between noise derivatives increases exponentially with the order of noise derivatives. Simulations show that derivatives above 6 can be neglected [14]. The generalized noise precision matrices are given by $\tilde{\Pi}_w = S(\sigma^2) \otimes \Pi_w$, $\tilde{\Pi}_z = S(\sigma^2) \otimes \Pi_z$ and $\tilde{\Pi}_v = S(\sigma^2) \otimes \Pi_v$, where Π_w, Π_z and Π_v are the inverse noise covariances.

C. Generalized motion of output and noises

The generalized motion of output $\tilde{\mathbf{y}}$ is practically not accessible for sensors. Moreover, most of the sensors like encoders operate with discrete measurements, unlike biophysical systems like the brain. Therefore, as a pre-processing step for estimation, $\tilde{\mathbf{y}}$ should be computed in discrete domain. Given the p temporal derivatives $\tilde{\mathbf{y}}$ at time t, the p output sequence surrounding $\mathbf{y}$ can be approximated using Taylor series as [14]:

$$\hat{\mathbf{y}} = \begin{bmatrix} .. \\ \mathbf{y}(t-dt) \\ \mathbf{y}(t) \\ \mathbf{y}(t+dt) \\ .. \end{bmatrix} = (E \otimes I_m)\tilde{\mathbf{y}},\ E_{ij} = \frac{[(i - \frac{p+1}{2})dt]^{j-1}}{(j-1)!}, \tag{5}$$

where $i, j = 1, 2, ...p+1$ and $\hat{y}$ has the size $m(p+1) \times 1$. Therefore, generalized motion of output $\tilde{\mathbf{y}}$ at time t is:

$$\tilde{\mathbf{y}} = (E^{-1} \otimes I_m)\hat{\mathbf{y}}. \tag{6}$$

Using $\tilde{\mathbf{y}}$ embeds more temporal information about the plant into the data in the form of conditional trajectories, with the disadvantage of a time latency of $\frac{p}{2}dt$ in estimation. The next section employs this generalized output along with the generative model for observer designs.

IV. STATE AND INPUT OBSERVER DESIGN

This section delineates the main contribution of the paper through two observer designs: with (i) known inputs and (ii) unknown inputs, for a general LTI system, and formulates the stability condition.

A. Observer design with unknown inputs

According to DEM, estimation is performed through a gradient ascent over the variational energy (variational component of free energy) with respect to hidden states and inputs [14]. With the mean-field approximation and Laplace approximation in place [7], the variational energy at time t is given by

$$V(t) = -\frac{1}{2}\tilde{\epsilon}^T\tilde{\Pi}\tilde{\epsilon}, \tag{7}$$

where $\tilde{\Pi} = diag(\tilde{\Pi}_z, \tilde{\Pi}_v, \tilde{\Pi}_w)$ is the generalized noise precision matrix, $\tilde{\epsilon}$ is the prediction error. The prediction error is formulated as:

$$\tilde{\epsilon}(t) = \begin{bmatrix} \tilde{\epsilon}^y \\ \tilde{\epsilon}^v \\ \tilde{\epsilon}^x \end{bmatrix} = \begin{bmatrix} \tilde{\mathbf{y}} - \tilde{C}\tilde{x} \\ \tilde{v} - \tilde{\eta} \\ D_x\tilde{x} - \tilde{A}\tilde{x} - \tilde{B}\tilde{v} \end{bmatrix}, \tag{8}$$

where $\tilde{\eta}$ is the prior belief of the inputs, which is crucial for observer design with unknown input. During fault detection in industrial automation processes, the expected inputs under normal conditions are known. This prior knowledge can be incorporated into the observer using $\tilde{\eta}$ with higher precision $\tilde{\Pi}_v$. For a completely unknown $\tilde{\eta}$, precision $\tilde{\Pi}_v$ should be set very low. Taking derivative of Equation 7 with respect to $X = [\tilde{x}, \tilde{v}]^T$ yields:

$$V(t)_X = -\tilde{\epsilon}_X^T\tilde{\Pi}\tilde{\epsilon}, \tag{9}$$

where

$$\tilde{\epsilon}_X(t) = \begin{bmatrix} \tilde{\epsilon}_{\tilde{x}}^{y} & \tilde{\epsilon}_{\tilde{v}}^{y} \\ \tilde{\epsilon}_{\tilde{x}}^{v} & \tilde{\epsilon}_{\tilde{v}}^{v} \\ \tilde{\epsilon}_{\tilde{x}}^{x} & \tilde{\epsilon}_{\tilde{v}}^{x} \end{bmatrix} = \begin{bmatrix} -\tilde{C} & O \\ O & I \\ D_x - \tilde{A} & -\tilde{B} \end{bmatrix}. \quad (10)$$

The update equation after *free-form* approximation [14] is expressed as a gradient ascent over the variational energy:

$$\dot{X} = \begin{bmatrix} k_x I_{n(p+1)} & O \\ O & k_v I_{r(d+1)} \end{bmatrix} V(t)_X + \begin{bmatrix} D_x & O \\ O & D_v \end{bmatrix} X, \quad (11)$$

where k_x and k_v are the learning rates for state and input update respectively. Substituting Equations 8, 9 and 10 in 11 upon simplification yields a linear observer design formulated as:

$$\dot{X} = \begin{bmatrix} \dot{\tilde{x}} \\ \dot{\tilde{v}} \end{bmatrix} = \begin{bmatrix} A_1 \\ A_2 \end{bmatrix} \begin{bmatrix} \tilde{x} \\ \tilde{v} \end{bmatrix} + \begin{bmatrix} B_1 \\ B_2 \end{bmatrix} \begin{bmatrix} \tilde{\mathbf{y}} \\ -\tilde{\eta} \end{bmatrix} \; and \; Y = X, \quad (12)$$

where Y is the output of the observer and,

$$A_1 = \begin{bmatrix} D_x & O \end{bmatrix} + k_x \begin{bmatrix} \tilde{C}^T \\ O \end{bmatrix} \begin{bmatrix} \tilde{\Pi}_z & O \\ O & \tilde{\Pi}_v \end{bmatrix} \begin{bmatrix} -\tilde{C} & O \\ O & I \end{bmatrix} - k_x (D_x - \tilde{A})^T \tilde{\Pi}_w \begin{bmatrix} D_x - \tilde{A} & -\tilde{B} \end{bmatrix},$$

$$A_2 = \begin{bmatrix} O & D_v \end{bmatrix} + k_v \begin{bmatrix} O & -I \end{bmatrix} \begin{bmatrix} \tilde{\Pi}_z & O \\ O & \tilde{\Pi}_v \end{bmatrix} \begin{bmatrix} -\tilde{C} & O \\ O & I \end{bmatrix} + k_v \tilde{B}^T \tilde{\Pi}_w \begin{bmatrix} D_x - \tilde{A} & -\tilde{B} \end{bmatrix},$$

$$B_1 = k_x \begin{bmatrix} \tilde{C}^T & O \end{bmatrix} \begin{bmatrix} \tilde{\Pi}_z & O \\ O & \tilde{\Pi}_v \end{bmatrix}, \; B_2 = k_v \begin{bmatrix} O & -I \end{bmatrix} \begin{bmatrix} \tilde{\Pi}_z & O \\ O & \tilde{\Pi}_v \end{bmatrix}$$

It can be observed from Equation 12 that the inputs and states can be recovered by using the output of plant $\tilde{\mathbf{y}}$ and prior for inputs $\tilde{\eta}$ as inputs to the observer. An exact algebraic discretization is used to numerically integrate the observer for estimation with time-sampled output $\mathbf{y}$.

B. Observer design with known inputs

DEM can be reformulated for state estimation with known inputs. When the inputs are known, the update rule for $\tilde{x}$ in Equation 12 can be rearranged as:

$$\dot{\tilde{x}} = \begin{bmatrix} D_x - k_x \tilde{C}^T \tilde{\Pi}_z \tilde{C} - k_x (D_x - \tilde{A})^T \tilde{\Pi}_w (D_x - \tilde{A}) \end{bmatrix} \tilde{x} + k_x \begin{bmatrix} \tilde{C}^T \tilde{\Pi}_z & (D_x - \tilde{A})^T \tilde{\Pi}_w \tilde{B} \end{bmatrix} \begin{bmatrix} \tilde{\mathbf{y}} \\ \tilde{v} \end{bmatrix} \quad (14)$$

The input to the linear state observer with known system inputs is the combined vector of generalized output and input of the system $[\tilde{\mathbf{y}}, \tilde{v}]^T$.

C. Stability condition for observer with unknown inputs

This section explicates the stability conditions for the observer design presented in Section IV-A. The error between observer's estimates and the ideal values from the plant is given by $\tilde{e} = \begin{bmatrix} \tilde{e}^x \\ \tilde{e}^v \end{bmatrix} = \begin{bmatrix} \tilde{\mathbf{x}} - \tilde{x} \\ \tilde{\mathbf{v}} - \tilde{v} \end{bmatrix}$. Taking the derivative of $\tilde{e}$ and substituting Equations 3 and 12 into it after simplification yields the error dynamics of the observer as:

$$\dot{\tilde{e}} = \begin{bmatrix} \dot{\tilde{e}}^x \\ \dot{\tilde{e}}^v \end{bmatrix} = A_3 \begin{bmatrix} \tilde{e}^x \\ \tilde{e}^v \end{bmatrix} \tilde{e} + A_4 \begin{bmatrix} \tilde{x} \\ \tilde{v} \end{bmatrix} + A_5 \begin{bmatrix} \tilde{w} \\ \tilde{z} \\ \tilde{\eta} \end{bmatrix}, \quad (15)$$

where A_3, A_4 and A_5 are given by Equation 13. Assuming that the states, inputs and noises for the system are bounded for a stable system under consideration, the error dynamics stabilizes if all the eigen values of A_3 have negative real part. Therefore, selecting the learning rates k_x and k_v such that A_3 represents a stable system matrix acts as the design criteria for a stable observer. Section VI-C deals with simulating the observer for a wide range of stable systems. The next section delineates the components of the observer design that contribute to its functioning.

V. COMPONENTS OF OBSERVER DESIGN

This section elucidates the relevance of main components of the observer by testing it on an LTI system given by:

$$A = \begin{bmatrix} -0.25 & 1.00 \\ -0.50 & -0.25 \end{bmatrix}, B = \begin{bmatrix} 1 \\ 0 \end{bmatrix}, C = \begin{bmatrix} 0.125 & 0.1633 \\ 0.125 & 0.0676 \\ 0.125 & -0.0676 \\ 0.125 & -0.1633 \end{bmatrix} \quad (16)$$

and quantifying the performance using sum of squared error (SSE) in state and input estimation. Parameters from [14] are adopted for a convenient result comparison. Unless mentioned otherwise, the same system will be used throughout the paper with an input of $v = e^{-0.25(t-12)^2}$, noise precisions $\Pi_w = e^8 I_{n \times n}$ and $\Pi_z = e^8 I_{m \times m}$, noise smoothness parameters (Equation 4) $\sigma = 0.5$, order of generalized motion $p = 6, d = 2$ and sampling time $dt = 0.1s$.

A. Generalized motion of output

The advantage of using generalized motion of the output $\mathbf{y}$ as discussed in Section III-C is illustrated in Figure 1 (for the system given above), which shows a better state estimation when generalized motion for $\mathbf{y}$ is used. Quantitatively, it corresponds to a drop in SSE for state estimation from *5.11* to *2.2* when generalized motion of output is used, thereby demonstrating its relevance.

$$A_3 = \begin{bmatrix} D_x - k_x (D_x - \tilde{A})^T \tilde{\Pi}_w (D_x - \tilde{A}) - k_x \tilde{C}^T \tilde{\Pi}_z \tilde{C} & k_x (D_x - \tilde{A})^T \tilde{\Pi}_w \tilde{B} \\ k_v \tilde{B}^T \tilde{\Pi}_w (D_x - \tilde{A}) & D_v - k_v \tilde{B}^T \tilde{\Pi}_w \tilde{B} - k_v \tilde{\Pi}_v \end{bmatrix}$$

$$A_4 = \begin{bmatrix} (-I + k_x (D_x - \tilde{A})^T \tilde{\Pi}_w)(D_x - \tilde{A}) & \tilde{B} - k_x (D_x - \tilde{A})^T \tilde{\Pi}_w \tilde{B} \\ -k_v \tilde{B}^T \tilde{\Pi}_w (D_x - \tilde{A}) & k_v \tilde{B}^T \tilde{\Pi}_w \tilde{B} + k_v \tilde{\Pi}_v \end{bmatrix}, \; A_5 = \begin{bmatrix} I & -k_x \tilde{C}^T \tilde{\Pi}_z & O \\ O & O & -k_v \tilde{\Pi}_v \end{bmatrix} \quad (13)$$

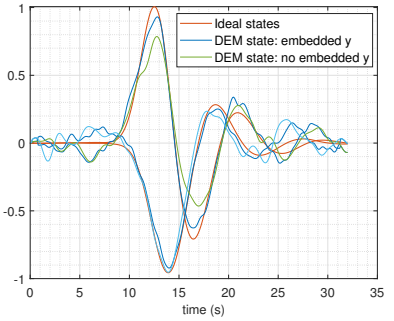

Fig 1: State estimation with and without embedding generalized motion to the output. The blue curve uses higher derivatives of y for state estimation, while the green curve doesn't. The blue is a better approximation of red than the green.

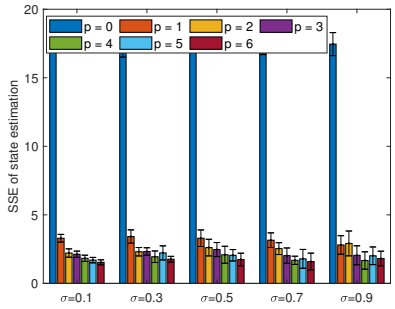

Fig 2: Embedding higher levels for the generalized motion of states decreases the state estimation error. The behaviour is robust against noise smoothness σ.

B. Embedding order of states and input

The embedding order represents the number of derivatives used in the generalized coordinates of the states and inputs. This section demonstrates the advantage of using generalized motion of states. Figure 2 and 3 shows the increasing accuracy of state and input estimation with increasing embedding order p for the states for the system given in Section V. The experiments were repeated for different noise smoothness σ to demonstrate the robustness of the method. In summary, a higher order p ensures better accuracy in state estimation. Similar results can be achieved for higher order embedding d of input on state and input estimation.

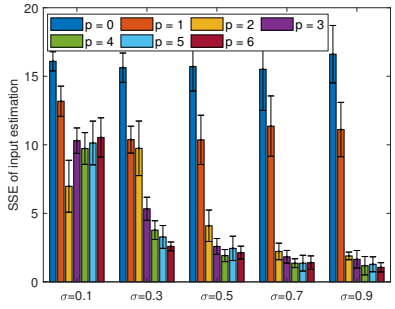

Fig 3: Higher order of generalized states increases the accuracy of input estimation for different noise smoothness σ. Input estimation is found to be less accurate for lower σ.

C. Accuracy V/S Complexity

Free energy can be defined as complexity minus accuracy [10], where complexity is the measure of closeness of the estimates to the prior information, while accuracy is the measure of sensory surprisal or the sensory prediction error. A higher Π_v favours a higher weightage for priors during inference, while a lower Π_v favours a higher weightage for incoming data. Figure 4 demonstrates DEM's input estimation for a constant inaccurate prior of 0.5 and varying Π_v. It shows that setting a low value for Π_v results in accurate input estimation, even with inaccurate prior η. Since accuracy is the focus of the paper, low value of Π_v will be used throughout.

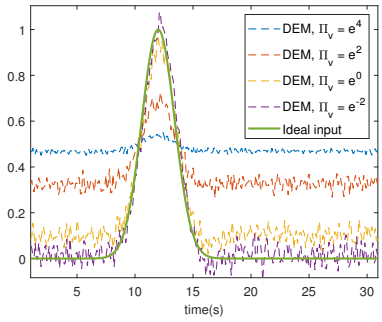

Fig 4: Setting low Π_v results in accurate input estimation even with wrong priors. An inaccurate constant prior of 0.5 was used with $\sigma = 0.01, \Pi_w = \Pi_z = e^{12}$.

D. Learning rates

The inference process of brain is modelled as a gradient ascent over the variational energy. Since DEM is a fixed-form approximation to the ensemble density that tracks the trajectory of conditional mode, an increase in learning rate results in an exponentially faster convergence of this trajectory to the conditional mode, thereby maximizing variational energy [14]. This results in a more accurate state and input estimation with increasing learning rate, which is demonstrated in Figure 5. It can be observed that a higher learning rate results in lower error in state estimation. Similar conclusion can be drawn for input estimation. Since discretization of the observer is exact, higher learning rates does not entail numerical instability as long as the selection criteria given in Section IV-C is met.

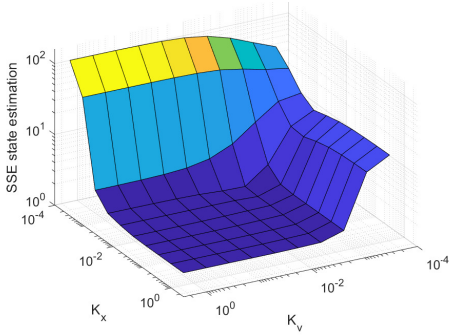

Fig 5: Higher learning rates result in better state estimation.

E. Equivalence of DEM with Kalman Filter

In case of white noise, the state estimation of DEM given in Equation 14 (without generalized motion) reduces to:

$$\dot{x} = k_x(-A^T\Pi_x A - C^T\Pi_y C)x - k_x(A^T\Pi_x)Bv + k_x C^T\Pi_y y. \tag{17}$$

This is very similar in form with the KF state update equation (with respect to variables x, v and y):

$$\dot{x} = (A - PC^T\Pi_y C)x + Bv + P(C^T\Pi_y)y, \tag{18}$$

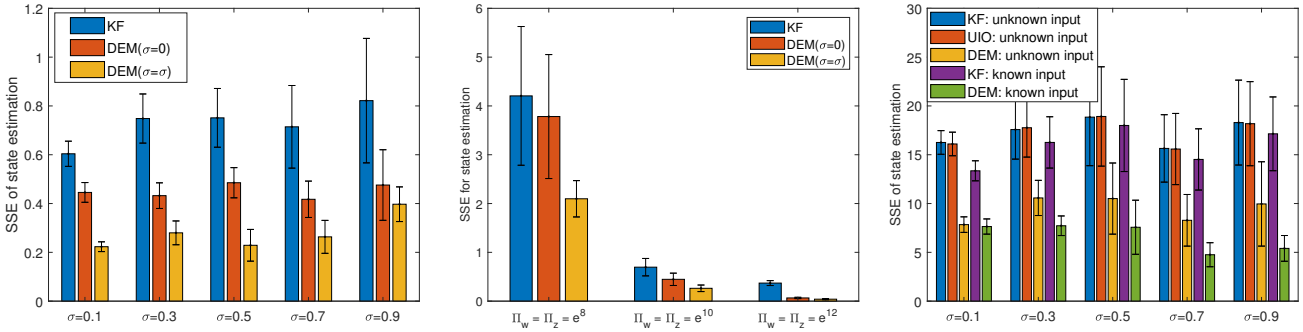

(a) Benchmark for noise smoothness. (b) Benchmark for noise variance. (c) Benchmark against other observers.

Fig. 6: Benchmarking observer for different noise smoothness and noise variance against KF and UIO.

where P is the error covariance that solves the Riccati equation $\dot{P} = AP + PA^T + \Pi_w^{-1} - PC^T\Pi_z^T CP^T$. If inputs are not modelled ($v = 0$ and $\Pi_x << \Pi_y$) and the learning rate k_x is tuned close to P ($k_x = P$), both the update equations 17 and 18 simplifies such that they behave exactly the same. Figure 7 shows the coinciding state estimation for DEM and KF for the same system given in Section V with $\sigma = 10^{-9}$, $dt = 0.5s$ and $\Pi_x = e^8 I_{2\times 2}$ (during data generation). A small precision of $\Pi_x = e^0 I_{2\times 2}$ is used while estimating with unmodelled v. Therefore, it can be concluded that DEM behaves like KF when noises are white and inputs are unmodelled. The next section deals with proving rigorously through simulations that when the noises are colored, DEM moves away from KF and outperforms KF and UIO.

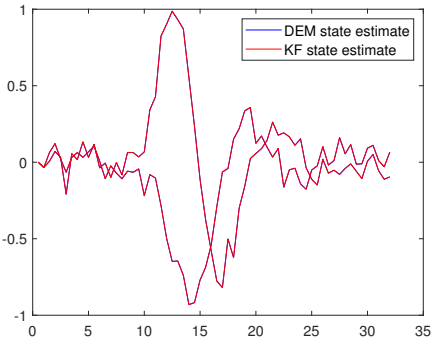

Fig 7: State estimation of KF and DEM coincides when noises are white and inputs are not modelled. Here Π_x is assumed to be $e^0 I_{2\times 2}$ during estimation. $\sigma = 10^{-9}$ and $dt = 0.5s$.

VI. BENCHMARK THE OBSERVER

This section aims to establish the superior performance of DEM against other benchmarks through a series of rigorous simulations under varied conditions.

A. Benchmark state observer

This section benchmarks the observer against KF and Unknown Input Observer (UIO) [3] for the system given in Equation 16. This version of UIO was selected owing to its capability to simultaneously estimate state and input without delays for a discrete LTI system. Correct noise smoothness value is key towards best inference. Figures 6a and 6b demonstrate the performance of DEM with unknown inputs for different levels of noise smoothness (with $\Pi_w = \Pi_z = e^{10}$) and noise variances (with $\sigma = 0.5$) respectively, where $DEM(\sigma = 0)$ assumes an unknown infinitely rough noise during estimation while $DEM(\sigma = \sigma)$ uses the known σ. DEM with known and unknown noise smoothness consistently outperforms KF for state estimation for varied noise smoothness and variance.

Given the correct noise smoothness and the system in Equation 16, 10 simulations each were used to generate Figure 6c with parameters from Section V and $dt = 0.02s$. It shows that DEM outperforms KF with lower SSE in state estimation, both for known and unknown input. Moreover, the performance of KF worsens as the noise smoothness increases. This can be attributed to the failed assumption of uncorrelated nature of the noise that KF is based upon. Modelling the states and inputs in the generalized coordinates embeds higher order motion during inference, motivating the use of DEM for state estimation while dealing with coloured noises.

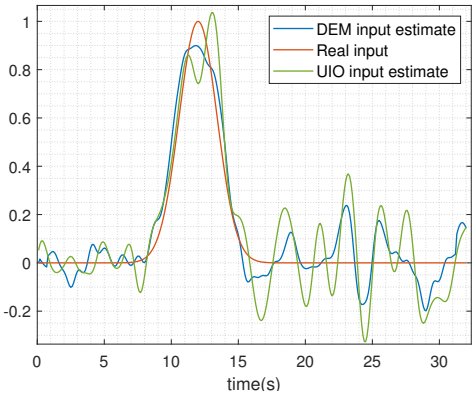

Fig 8: Gaussian bump input estimated by DEM and UIO. DEM provides a better input estimate than UIO.

B. Benchmark input observer

This section benchmarks unknown input estimation given by Equation 12 against UIO. Figure 8 shows the successful input estimation by DEM and UIO for the system given in Equation 16 with $dt = 0.02s$. Input estimate from DEM is more similar to the ideal input when compared to the estimation from UIO. The mean SSE for 10 such simulations each

for different noise smoothness is plotted with one standard deviation as shown in Figure 9. It can be observed that DEM outperforms UIO for input estimation under highly coloured noises. Better performance of DEM can be attributed to the tracking of trajectories of inputs through generalized coordinates, unlike just the point estimates by UIO.

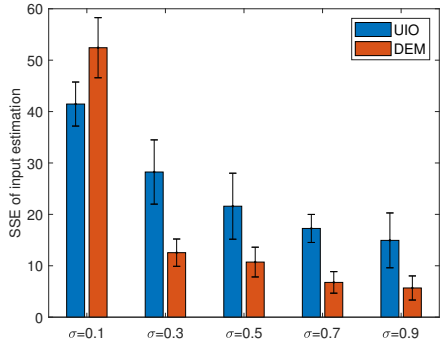

Fig 9: DEM outperforming UIO for input estimation under high noise smoothness.

C. Fully randomized benchmarking

This section establishes the superior performance of DEM by generalizing it over a wide range of systems with different input signals. System matrices A, B and C were randomized for values in the range [-1,1] with 2 state variables and randomly selected number of outputs ranging between 1 and 6. Noise variances $\Pi_w = e^6 I_{n\times n}$ and $\Pi_z = e^6 I_{m\times m}$ were used with a noise smoothness of 0.5. To preclude high SSE in state estimation, only stable A matrices were chosen . 100 simulations each for three different input signals - Gaussian $(e^{-0.25(t-12)^2})$, sinusoidal $(\sin 0.25t)$ and ramp $(t/32)$ - were used for a performance comparison. Figure 10 shows all the instances with known inputs. Most of the samples occupy the lower diagonal half of Figure 10, indicating that DEM outperforms KF in most cases with coloured noise by reducing the sum of squared error (SSE) in state estimation for a wide range of randomly generated LTI systems for different known inputs. In summary, DEM outperforms other benchmarks in state and input estimation for randomised noise smoothness, noise variance, systems and input signals. The next section demonstrates the applicability of the observer on real systems.

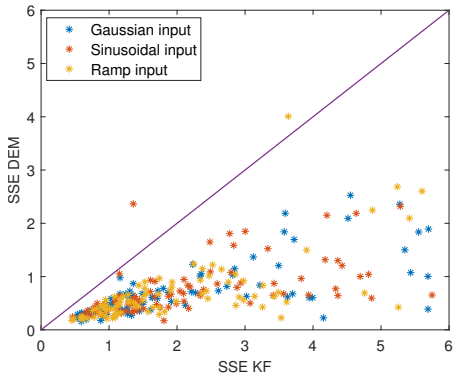

Fig 10: DEM outperforms KF for state estimation with known inputs. Coloured noises and three inputs were applied on 300 randomly generated systems to plot the estimation error.

VII. PROOF OF CONCEPT ON REAL SYSTEM

This section aims to provide a proof of concept for the observer design with the help of data acquired from a maxon DC motor. The linear state space equation of a DC motor is:

$$\dot{x} = \begin{bmatrix} \dot{\theta} \\ \ddot{\theta} \\ \dot{i} \end{bmatrix} = \begin{bmatrix} 0 & 1 & 0 \\ 0 & -\frac{b}{J} & \frac{K}{J} \\ 0 & -\frac{K}{L} & -\frac{R}{L} \end{bmatrix} \begin{bmatrix} \theta \\ \dot{\theta} \\ i \end{bmatrix} + \begin{bmatrix} 0 \\ 0 \\ \frac{1}{L} \end{bmatrix} V$$
$$y = \begin{bmatrix} 1 & 0 & 0 \end{bmatrix} \begin{bmatrix} \theta \\ \dot{\theta} \\ i \end{bmatrix}, \tag{19}$$

where θ is the angular position of the rotating motor knob, i the current, $b = 3.74 \times 10^{-5} Nms$ the damping ratio, $J = 2.69 \times 10^{-4} kgm^2$ the moment of inertia of the rotor, $K = 0.0472 Vrad^{-1}s^{-1}$ the electromotive force constant, $L = 8.4 \times 10^{-4} H$ the inductance, and $R = 9.24\Omega$ the resistance. The input to the system is voltage, while the output is the angular position of the knob.

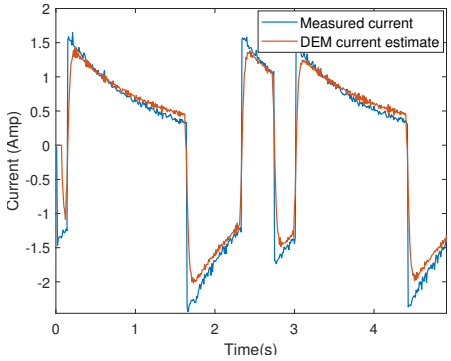

Fig 11: Current estimation using DEM in red is similar to the measured motor current in blue. Slight deviation is due to the imperfect motor parameters.

The output data acquired for varying input was used for inference by the proposed observer. The results of the state and input estimation is shown in Figure 11 and 12 respectively. It can be observed that DEM estimates for current and voltage closely resemble the measurements respectively. The SSE for state estimation is then computed. DEM, has a lower SSE for state estimation of 8809, when compared to 14800 and 2.6×10^6 as that of UIO and KF respectively (overlapping plots were omitted for visibility). Therefore, DEM can effectively be used for state and input estimation on real systems with noises. MATLAB codes are available at $www.github.com/ajitham123/DEM\_observer$.

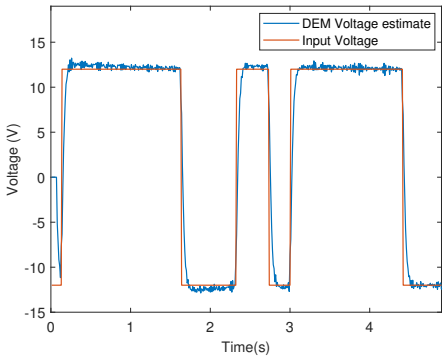

Fig 12: The input voltage estimation of DEM in blue is similar to the measured voltage in red, demonstrating that the observer works on real systems.

VIII. CONCLUSIONS AND FUTURE WORK

The paper introduced a brain inspired state and input observer based on DEM that can be applied to general LTI systems. The observer leverages the information contained within coloured noises through generalized coordinates. Extensive simulations with coloured noises show that the observer outperform state-of-the-art observers through minimal state and input estimation errors. The observer was generalized for a wide range of system parameters, noise smoothness, noise variance and input signals. Finally, the proof of concept was provided through state and input estimation on a real system, demonstrating its real life performance. The main drawback of the observer is the poor input estimation for low noise smoothness. Future work will concentrate on extending the observer for complex hierarchical systems.

ACKNOWLEDGMENT

We thank Prof. Robert Babuska for providing us with the motor data. We also thank Karl Friston and Sherin Grimbergen for the insightful discussions on FEP.

REFERENCES

[1] J. Chen, R. J. Patton, and H.-Y. Zhang, "Design of unknown input observers and robust fault detection filters," *International Journal of control*, vol. 63, no. 1, pp. 85–105, 1996.

[2] M. Darouach, M. Zasadzinski, A. B. Onana, and S. Nowakowski, "Kalman filtering with unknown inputs via optimal state estimation of singular systems," *International journal of systems science*, vol. 26, no. 10, pp. 2015–2028, 1995.

[3] B. A. Charandabi and H. J. Marquez, "Observer design for discrete-time linear systems with unknown disturbances," in *2012 IEEE 51st IEEE Conference on Decision and Control (CDC)*. IEEE, 2012, pp. 2563–2568.

[4] H. Kuhlmann, "Kalman-filtering with coloured measurement noise for deformation analysis," in *Proceedings, 11th FIG Symposium on Deformation Measurements, Santorini, Greece*, 2003.

[5] K. Wang, Y. Li, and C. Rizos, "Practical approaches to kalman filtering with time-correlated measurement errors," *IEEE Transactions on Aerospace and Electronic Systems*, vol. 48, no. 2, pp. 1669–1681, 2012.

[6] K. Friston, "The free-energy principle: a unified brain theory?" *Nature reviews neuroscience*, vol. 11, no. 2, p. 127, 2010.

[7] C. L. Buckley, C. S. Kim, S. McGregor, and A. K. Seth, "The free energy principle for action and perception: A mathematical review," *Journal of Mathematical Psychology*, vol. 81, pp. 55–79, 2017.

[8] J. Hohwy, *The predictive mind*. Oxford University Press, 2013.

[9] K. Friston, "The free-energy principle: a rough guide to the brain?" *Trends in cognitive sciences*, vol. 13, no. 7, pp. 293–301, 2009.

[10] K. J. Friston, J. Daunizeau, J. Kilner, and S. J. Kiebel, "Action and behavior: a free-energy formulation," *Biological cybernetics*, vol. 102, no. 3, pp. 227–260, 2010.

[11] R. L. Carhart-Harris and K. J. Friston, "The default-mode, ego-functions and free-energy: a neurobiological account of freudian ideas," *Brain*, vol. 133, no. 4, pp. 1265–1283, 2010.

[12] K. J. Friston, J. Daunizeau, and S. J. Kiebel, "Reinforcement learning or active inference?" *PloS one*, vol. 4, no. 7, p. e6421, 2009.

[13] K. Friston, "Hierarchical models in the brain," *PLoS computational biology*, vol. 4, no. 11, p. e1000211, 2008.

[14] K. J. Friston, N. Trujillo-Barreto, and J. Daunizeau, "DEM: a variational treatment of dynamic systems," *Neuroimage*, vol. 41, no. 3, pp. 849–885, 2008.

[15] L. Ma, H. Wang, and J. Chen, "Analysis of kalman filter with correlated noises under different dependence," *JOURNAL OF INFORMATION &COMPUTATIONAL SCIENCE*, vol. 7, no. 5, pp. 1147–1154, 2010.

[16] A. Bryson and D. Johansen, "Linear filtering for time-varying systems using measurements containing colored noise," *IEEE Transactions on Automatic Control*, vol. 10, no. 1, pp. 4–10, 1965.

[17] A. Bryson Jr and L. Henrikson, "Estimation using sampled data containing sequentially correlated noise." *Journal of Spacecraft and Rockets*, vol. 5, no. 6, pp. 662–665, 1968.

[18] D. Simon, *Optimal state estimation: Kalman, H infinity, and nonlinear approaches*. John Wiley & Sons, 2006.

[19] J. L. Crassidis and J. L. Junkins, *Optimal estimation of dynamic systems*. CRC press, 2011.

[20] S. Z. Yong, M. Zhu, and E. Frazzoli, "Simultaneous input and state estimation for linear time-varying continuous-time stochastic systems," *IEEE Transactions on Automatic Control*, vol. 62, no. 5, pp. 2531–2538, 2016.

[21] C. Pezzato, R. M. Ferrari, and C. Hernandez, "A novel adaptive controller for robot manipulators based on active inference," *IEEE Robotics and Automation Letters*, 2020.

[22] P. Lanillos and G. Cheng, "Adaptive robot body learning and estimation through predictive coding," in *2018 IEEE/RSJ International Conference on Intelligent Robots and Systems (IROS)*. IEEE, 2018, pp. 4083–4090.